Earth System
Science
Data

Open Access

Discussions

Long-term Land-Atmosphere Energy and Water Exchange Observational Dataset over central Tibetan Plateau

1

2   Haipeng Yu[1], Guantian Wang[1,4], Zeyong Hu[1]*, Yaoming Ma[2], Maoshan Li[3], Weiqiang Ma[2], Lianglei

3   Gu[1], Fanglin Sun[1], Hongchun Gao[1], Shujin Wang[1], Fuquan Lu[1,4]

4

5

6   [1] Nagqu Plateau Climate and Environment Observation and Research Station of Tibet Autonomous

7   Region, State Key Laboratory of Cryospheric Science and Frozen Soil Engineering, Northwest Institute

8   of Eco-Environment and Resources, Chinese Academy of Sciences, Lanzhou 730000, China

9   [2]Land-Atmosphere Interaction and Its Climatic Effects Group, State Key Laboratory of Tibetan Plateau

10   Earth System, Environment and Resources, National Observation and Research Station for

11   Qomolongma Special Atmospheric Processes and Environmental Changes, Institute of Tibetan Plateau

12   Research, Chinese Academy of Sciences, Beijing 100101, China

13   [3]School of Atmospheric Sciences, Plateau Atmosphere and Environment Key Laboratory of Sichuan

14   Province, Chengdu Plain Urban Meteorology and Environment Observation and Research Station of

15   Sichuan Province, Chengdu University of Information Technology, Chengdu 610225, China

16   [4]University of Chinese Academy of Sciences, Beijing 100049, China

17

18   *Correspondence to*: Zeyong Hu (zyhu@lzb.ac.cn)

19

20   **Abstract**：In recent decades, the climate of Tibetan Plateau has undergone notable changes, which has

21   a strong influence on global climate systems and human activities, making it a research hotspot.

22   However, due to its extreme elevation, harsh environment, and complex underlying surface, long-term

23   observations of the central Plateau's atmospheric vertical profiles have been challenging and scientific

24   data sharing is crucial and in urgent need. This paper presents a 9-year observational dataset (2014-

25   2022) with hourly temporal resolution from the Nagqu region of northern Tibet. The dataset is a

26   combination of four field stations covering the central Tibetan Plateau, which recorded near-surface

27   meteorological data, radiation budget, turbulent fluxes, and soil hydrothermal characteristics. All

28   observational items in this dataset underwent data processing and quality control to ensure data quality.

29   This dataset represents the most detailed raw observational data on the central Tibetan Plateau's spatial

30   coverage and recent changes. It holds significant value in revealing energy and water exchanges

31   between the land surface and the atmosphere on the Tibetan Plateau. Main datasets are freely available

32   at   the   National   Tibetan   Plateau   /   Third   Pole   Environment   Data   Center

33   (https://doi.org/10.11888/Meteoro.tpdc.270010, Hu et al., 2019) and additionally at National Tibetan

34   Plateau / Third Pole Environment Data Center (https://doi.org/10.11888/Atmos.tpdc.300325, Wang et

35   al., 2023).

36

37   **Key words:** field observation, observational dataset, land-atmosphere interaction, Tibetan Plateau,

38   energy and water exchanges

39

40   **1.Introduction**

41   The Tibetan Plateau (TP), with an average altitude exceeding 4000 meters, is the world's largest

42 mountain range, often referred to as the "Third Pole" (Qiu, 2008). It is the source of many major rivers,
43 including the Yangtze, Yellow, Mekong, and Brahmaputra, which provide freshwater to 1.4 billion
44 people (Immerzeel et al., 2020). It is also known as the "Asian Water Tower" (Immerzeel et al., 2010).
45 The plateau's substantial absorption of solar radiation renders it the warmest region in the mid-
46 troposphere. This plays a key role in the evolution of the East Asian Summer Monsoon and Indian
47 Summer Monsoon systems (Wu et al., 2007; Wu et al., 2012; Li et al., 2018; Zhang et al., 2019), which
48 in turn affect circulation patterns in East Asia, and even the Northern Hemisphere (Fan et al., 2023;
49 Curio and Scherer, 2016; Sun et al., 2022). The intricate surface characteristics of the TP make it
50 particularly susceptible to external disturbances in the context of global warming (Li et al., 2022; Kang
51 et al., 2010). Meteorological observations indicate that surface warming on the TP commenced at an
52 earlier and more accelerated pace than in other regions at the same latitude (Liu and Chen, 2000).
53 Climate change on the TP has resulted in most regions becoming warmer and moister, while the
54 southern part has become warmer and drier (Yang et al., 2014). These changes in temperature and
55 moisture have further led to significant shifts in many environmental systems on the plateau, including
56 precipitation (Yang et al., 2011), glaciers (Yao et al., 2012), lakes (Lei et al., 2014), and vegetation
57 (Shen et al., 2015). Therefore, in-depth research on TP not only helps us better understand the impact
58 of global warming on its unique ecosystems and climatic features, but also is crucial for assessing its
59 contribution to regional and even global water cycles and energy balance. In recent decades, a
60 multitude of comprehensive observation stations have been established with the objective of
61 strengthening climate change research on the TP. These include the Third Pole Environment
62 Observation and Research Platform and the Integrated Three-Dimensional Observation Research
63 Platform for Third Pole Environment (Ma et al., 2018; Ma et al., 2023). The establishment of these
64 observation stations has resulted in a significant improvement in the availability of data on land-
65 atmosphere interactions on the plateau. The comprehensive data network has enhanced the quality of
66 land surface models and corrected satellite retrievals (Ma et al., 2023). However, due to factors such as
67 transportation and maintenance costs, most observations are concentrated in the eastern part of the TP,
68 with limited long-term observations of the plateau's interior, especially in the high-altitude regions of
69 northern Tibet (Shen and Xiong,2016; Duan and Xiao, 2015).

70   The central Tibetan Plateau (CTP) belongs to a typical plateau climate with an average altitude
71 exceeding 4500 metres. It is bordered by the Kunlun and Tanggula Mountains to the northwest and the
72 Nyenchen Tanglha Mountains to the south, covering an area of 446,000 square kilometres, which
73 represents one-fifth of the total area of Tibet. The CTP is known as the "Roof of the Roof of the
74 World," representing the highest and most typical plateau form on the TP. Due to its high altitude, the
75 substrate is dominated by cold-resistant vegetation, with an annual precipitation of 154.9 mm and
76 approximately 50 rainy days, characterizing a typical subarctic semi-arid monsoon climate (Li et al.,
77 2017). During clear weather, the downward shortwave radiation peaks at 1200 W/m², which is
78 significantly higher than inland observations (He et al., 2010). The period from May to September is
79 characterised by warm and moist conditions, with frequent rainfall, while October to April is cold and
80 dry with prevalent strong winds. During the summer months, the CTP serves as a thermal core area,
81 with surface heating being a key factor in making the plateau a heat source. The thermal effect of the
82 CTP influences not only the plateau itself but also weather and climate systems in East Asia, and even
83 the Northern Hemisphere (Zhao et al.,2019). Over the past 40 years, the warming trend on the CTP has
84 been significantly higher than in lower-altitude areas, with surface temperature warming rates and
85 precipitation amounts also higher than in eastern regions of the TP (Chen et al., 2003; Liu et al., 2009;

86	Yang et al., 2002). The number of consecutive dry days on the central TP has been steadily decreasing
87	in conjunction with accelerated warming and moistening (Ciwangdunzhu et al., 2018), while its lakes
88	are experiencing strong expansion or contraction (Zhang et al., 2019; Lei et al., 2013 Lei et al., 2014).
89	Some lakes serve as heat sources year-round and have an annual evaporation rate of 312.9mm (Guo et
90	al., 2014). Concurrently, glaciers on the CTP are rapidly melting, and permafrost areas are shrinking,
91	severely impacting the surrounding environment (Jin et al., 2009; Sun et al., 2020). A substantial
92	evidence base indicates that the CTP 's ecological environment is highly fragile, and the surface heat
93	exchange in this region is significant for climate change. However, there remains substantial
94	uncertainty regarding the impact mechanisms (Song et al., 2012; Yang et al., 2014). This can be
95	attributed to the harsh environment, frequent extreme weather such as strong winds and hail showers,
96	and faulty observation equipment. Furthermore, much of the region's intricate topography is unsuitable
97	for human habitation, resulting in a sparsely populated area, inadequate transportation infrastructure,
98	and delayed equipment maintenance. This has led to the availability of relatively limited long-term and
99	stable observational data for the CTP.
100	To fill these gaps, a series of mesoscale observation networks have been established in the vicinity
101	of the Nagqu Observation Network of Plateau Climate and Environment (NPCE) (Xu et al., 2013). The
102	NPCE commenced observations in 1997 and serves as a link between the East Asian Monsoon and the
103	Indian Monsoon, as well as a transition zone between the monsoon systems and westerly circulation. It
104	is a region of significant thermal activity on the plateau, and the central zone for China's Third
105	Atmospheric Science Experiment on the TP. This distinctive geographical position gives NPCE a
106	pivotal role in TP research. Following decades of observations, data from the Nagqu observing network
107	has become an important platform for research on land-atmosphere interactions in northern Tibet. It has
108	provided significant support for studies on boundary layer observations (Gu et al., 2022; Ueno et al.,
109	2012), land-atmosphere energy transfer (Yang et al., 2010; Gu et al., 2015; Li et al., 2015), substrate
110	evaporation (Zou et al., 2018), soil hydrothermal balance (Bian et al., 2012; Fu et al., 2022), and
111	numerical simulations (Deng et al., 2021; Li et al., 2009; Sun et al., 2020). In recent years, there has
112	been a gradual increase in the availability of field datasets to the public with free access. In order to
113	optimise the potential value of scientific datasets, we describe and provide a high-time-resolution
114	dataset. This dataset comprises nine years of near-surface meteorological, radiation, turbulent flux, and
115	soil hydrothermal observations from NPCE. It provides a more accurate and comprehensive depiction
116	of land-atmosphere interactions and boundary layer structure on the TP, playing a key role in numerical
117	simulations and climate assessments.
118	The paper is organized as follows: Section 2 provides an overview of NPCE's geographic location,
119	observation equipment, variables, data processing, and data availability. Section 3 presents near-surface
120	meteorological, radiation, turbulent flux, and soil hydrothermal observations, discussing data integrity.
121	Section 4 comprises a discussion, and Section 5 is conclusion.
122	
123	**2. Observation network and data processing**
124	**2.1 Site descriptions**
125	The NPCE is affiliated with the Northwest Institute of Eco-Environment and Resources, Chinese
126	Academy of Sciences, was established on 4 May 2009, with observational activities commencing on 1
127	April 1997. The central station is situated in Niaoqu Village, Luoma Town, Seni District, Nagqu City,
128	Tibet Autonomous Region (longitude 91.90° E, latitude 31.37° N, altitude 4509 metres), near the
129	Tanggula Mountains, where the Indian monsoon and the East Asian monsoon intersect. The

130 observation field is relatively flat and open, with abundant water resources and situated in an area
131 characterised by pastoral activities. The substrate vegetation is primarily alpine grassland, with a
132 relatively clean atmosphere and a low aerosol content. The station's unique geographic location and
133 subsurface characteristics are significant for the observation and study of high-altitude climate
134 environments.
135   Over more than 20 years, NPCE has developed into a network of four atmospheric boundary layer
136 physics and land surface process observation points in the Nagqu region and along the Qinghai-Tibet
137 Highway. The locations in Figure 1 are BJ/Nagqu, Amdo, NewD66/Kekexili, and MS3478/Liangdaohe.
138 These represent different substrate characteristics, namely plateau grassland, plateau meadow, plateau
139 wetland, and plateau bareland. In 2014, NPCE became a member of the Chinese Academy of Sciences
140 Cold Region Surface Process and Environmental Monitoring Research Network and the Chinese
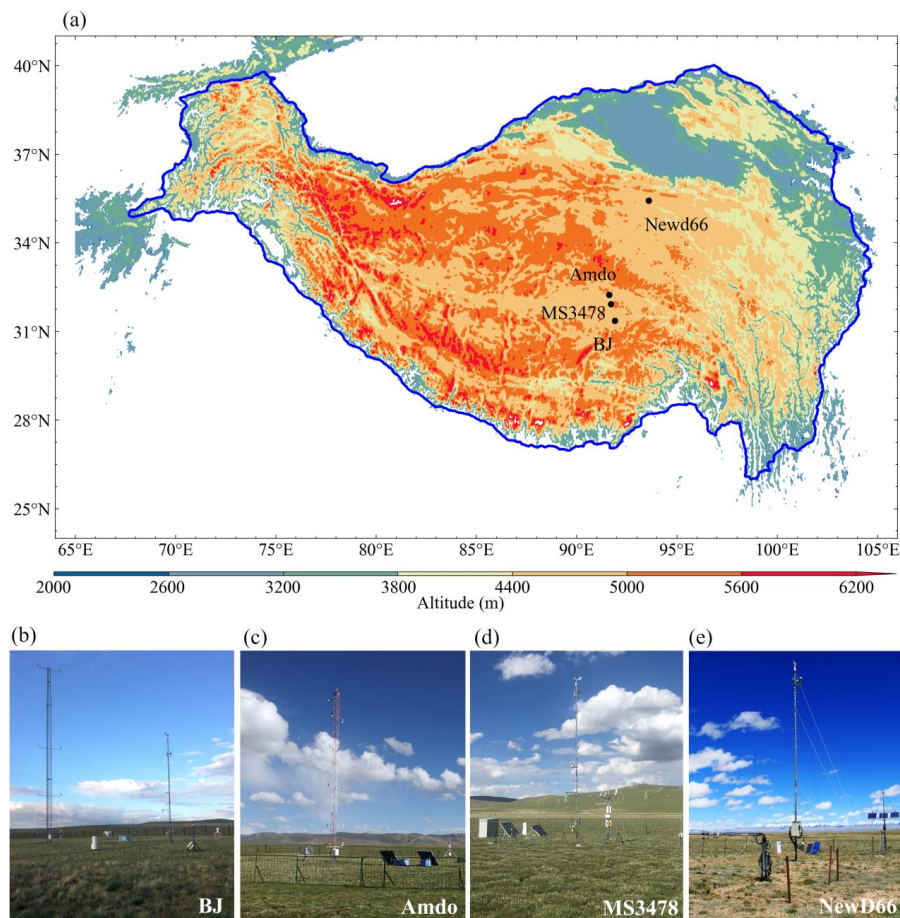141 Academy of Sciences Land Surface Process Research Network.

142

143

144   Figure 1. Geographic locations of the observation stations of NPCE (a) and on-site image of BJ (b),
145   Amdo (c), MS3478 (d), and NewD66 (e).

146

2.2 Observation infrastructure and data processing

The NPCE utilises automatic observation mode, capable of sustaining continuous observation throughout the year. In order to ensure the continuity and accuracy of the observation data, the maintenance engineers are responsible for conducting on-site inspections and maintenance of the infrastructures at regular intervals at each observation station and collect the observation data. All data are transmitted to the data centre for processing to facilitate timely and effective detection of technical problems.

The NPCE near-surface meteorological observation system consists of Planetary Boundary Layer (PBL) towers and Automatic Weather Stations (AWS). These instruments measure vertical profiles of meteorological conditions, including air temperature, relative humidity, wind direction and wind speed within the boundary layer. Observation heights range from 0.75-12 m at BJ and Amdo, and approximately 1 m and 10 m at NewD66 and MS3478. The observation probes deployed at each station were of the same type to ensure consistency, but the specific observation heights varied slightly across different stations. The vertical soil hydrothermal characteristics were measured at each station with multilayer soil temperature and moisture probes located between 5-160 cm from the surface, with a proportional distribution of observation depths. High-frequency Eddy Covariance (EC) systems were installed at the four stations after 2012, allowing for the capture of sensible, latent and carbon dioxide fluxes, with a sampling frequency of 0.1 s and an output interval of 30 minutes. Surface observations encompass surface air temperature, humidity, radiative quadrature, atmospheric pressure, precipitation, and snow depth. All observations are recorded at a sampling frequency of 10 seconds and an output interval of 30 minutes. More details of the observation instruments are listed in Table 1. Station BJ is also equipped with a ground-based microwave radiometer, a blowing snow observation instrument, and a wind profile radar. The ground-based microwave radiometer (MWP967KV) can observe temperature and humidity profiles up to 10 km above the surface under all weather conditions, with a 2-minute output interval. The FlowCapt FC4 blowing snow sensor inverts digital signals by collecting the acoustic pressure of the blowing snow particles as they impact. The CFL-03 pulsed Doppler wind profile radar (WPR) can capture the wind speed and wind direction profile. It has a detection range of 300 to 3,000 metres and an output interval of 5 minutes. These observational instruments collectively constitute a well-established monitoring system capable of comprehensively tracking weather events across the central TP and their associated impacts.

For near-surface micrometeorological observations in complex environments, quality control of data processing is crucial. In order to ensure the consistency of data at each site in the harsh natural environment of the TP, engineers firstly check the data in terms of range, which is a constant value set according to the climatic conditions of the TP and ignore the seasonal variations. Factors such as the replacement of original parts and extreme weather can lead to temporary sensor malfunction. This can result in no change or unrealistic jumps in the data for several hours. These factors can make it difficult to properly deal with the issue during the range check. Consequently, engineers will utilise manual quality control at the conclusion of the process, based on empirical observations, to rectify or eliminate anomalous intervals and thereby ensure that outliers do not adversely affect the mean observations. The removed missing measurements and outliers are denoted by NAN or -9999. Moreover, three categories of quality classification are employed for turbulent fluxes. 0 denotes the highest quality of flux, 1 denotes flux suitable for general analysis, and 2 denotes flux with possible anomalies.

Table 1. Detailed information about observation stations and instruments of NPCE.

Site	Variables	Sensor models	Manufacturers	Observation	Installation height/depth (m)	Units

Station	Variable	Model	Manufacturer	period	Height/Depth	Units
BJ Lat: 31.37°N Lon: 91.90°E Altitude: 4509 m Established in 2001 Plateau Grassland	Air temperature	HMP45D	Vaisala	2001-2018	1.0/2.0/4.0/8.0/16.0/24.0	°C
		HMP155	Vaisala	2012-2022	0.75/1.5/3.0/6.0/12.0/22.0	
	Wind speed and direction	A-5400	Komatsu	2001-2018	10.36	m/s
		WindSonic	Gill	2012- 2022	0.75/1.5/3.0/6.0/12.0/22.0	
	Relative humidity	HMP45D	Vaisala	2001-2018	1.0/2.0/4.0/8.0/16.0/24.0	%
		HMP155	Vaisala	2012-2022	0.75/1.5/3.0/6.0/12.0/22.0	
	Precipitation	NOAH-II	ETI	2001-2018	1.00	mm
		T-200B	Geonor	2012-2022	1.00	
	Soil temperature	TS-301	Okazaki	2001-2018	-0.04/-0.10/-0.20/-0.40	°C
		TR-219	Truwel	2012-2022	-0.05/-0.10/-0.20/-0.40/-0.80/-1.60	
	Soil volumetric water content	Trime EZ	IMKO	2001-2018	-0.04/-0.20	m³/m⁻³
		CS616	Campbell	2012-2022	-0.05/-0.10/-0.20/-0.40/-0.80/-1.60	
	Pressure	PTB220C	Vaisala	2001-2022	0.50	hPa
	Downward shortwave radiation	CM21	Kipp&Zonen	2001-2022	1.50	W/m⁻²
	Upward shortwave radiation	CM21	Kipp&Zonen	2001-2022	1.50	W/m⁻²
	Downward longwave radiation	PIR	Eppley	2001-2022	1.50	W/m⁻²
	Upward longwave radiation	PIR	Eppley	2001-2022	1.50	W/m⁻²
	Surface sensible heat flux	CSAT3	CAMPBELL	2008-2022	3.00	W/m⁻²
	Surface latent heat flux	LI7500A HMP45AC	CAMPBELL VAISALA			
Amdo Lat: 32.24°N Lon: 91.62°E Altitude: 4695 m Established in 1997 Plateau Meadow	Air temperature	HMP155	Vaisala	2012-2022	1.5/3.0/6.0/12.0	°C
	Wind speed and direction	WindSonic	Gill	2012-2022	1.5/3.0/6.0/12.0	m/s
	Relative humidity	HMP155	Vaisala	2012-2022	1.5/3.0/6.0/12.0	%
	Precipitation	T-200B	Geonor	2012-2022	1.00	mm
	Soil temperature	TR-219	Truwel	2012-2022	-0.05/-0.10/-0.20/-0.40/-0.80/-1.60	°C
	Soil volumetric water content	CS616	Campbell	2012-2022	-0.05/-0.10/-0.20/-0.40/-0.80/-1.60	m³/m⁻³
	Pressure	PTB220C	Vaisala	2001-2022	0.50	hPa
	Downward shortwave radiation	MS-801	EKO	2012-2022	1.50	W/m⁻²
	Upward shortwave radiation	MS-801	EKO	2012-2022	1.50	W/m⁻²
	Downward longwave radiation	PIR	EPPLEY	2012-2022	1.50	W/m⁻²
	Upward longwave radiation	PIR	EPPLEY	2012-2022	1.50	W/m⁻²
	Surface sensible heat flux	CSAT3	CAMPBELL	2012-2022	3.00	W/m⁻²
	Surface latent heat flux	LI7500A HMP45AC	CAMPBELL VAISALA			
MS3478 Lat: 31.93°N Lon: 91.71°E Altitude: 4620 m Established in 2001 Plateau Wetland	Air temperature	HMP45D	Vaisala	2001-2022	0.85/9.35	°C
	Wind speed and direction	A-5400	Komatsu	2001-2022	10.35	m/s
	Relative humidity	HMP45D	Vaisala	2001-2022	0.85/9.35	%
	Precipitation	NOAH-II	ETI	2001-2022	1.00	mm
	Soil temperature	TS-301	Okazaki	2001-2022	-0.04/-0.10/-0.20/-0.40	°C
	Soil volumetric water content	Trime EZ	IMKO	2001-2022	-0.04/-0.20	m³/m⁻³
	Pressure	PTB220C	Vaisala	2001-2022	0.5	hPa
	Downward shortwave radiation	CM21	Kipp&Zonen	2001-2022	1.50	W/m⁻²
	Upward shortwave radiation	CM21	Kipp&Zonen	2001-2022	1.50	W/m⁻²
	Downward longwave radiation	PIR	Eppley	2001-2022	1.50	W/m⁻²
	Upward longwave radiation	PIR	Eppley	2001-2022	1.50	W/m⁻²
	Surface sensible heat flux	CSAT3	CAMPBELL	2012-2022	3.00	W/m⁻²
	Surface latent heat flux	LI7500A HMP45AC	CAMPBELL VAISALA			
NewD66 Lat: 35.43°N Lon: 93.59°E Altitude: 4465 m Established in 1997 Relocate in 2006 Plateau Bareland	Air temperature	HMP45D	Vaisala	1997-2022	0.60/9.30	°C
	Wind speed and direction	W955-FE	Komatsu	1997-2022	10.40	m/s
	Relative humidity	HMP45D	Vaisala	1997-2022	0.60/9.30	%
	Precipitation	NOAH-II	ETI	1997-2022	1.00	mm
	Soil temperature	TS-301	Okazaki	1997-2022	0.00/-0.01/-0.02/-0.03/-0.04/-0.06/-0.08/-0.10/-0.15/-0.20/-0.40/-0.60/-0.80/-1.00/-1.30/-1.60/-2.00/-2.12	°C
	Soil volumetric water content	Trime EZ	IMKO	1997-2022	-0.011/-0.04/-0.075/-0.20/-0.40/-0.60/-0.80/-1.00/-1.60/-2.06	m³/m⁻³
	Pressure	PTB210	Vaisala	1997-2022	0.5	hPa
	Downward shortwave radiation	CM21	Kipp&Zonne	1997-2022	1.50	W/m⁻²
	Upward shortwave radiation	CM21	Kipp&Zonne	1997-2022	1.50	W/m⁻²
	Downward longwave radiation	PIR	Eppley	1997-2022	1.50	W/m⁻²
	Upward longwave radiation	PIR	Eppley	1997-2022	1.50	W/m⁻²
	Surface sensible heat flux	CSAT3	CAMPBELL	2012-2022	3.00	W/m⁻²
	Surface latent heat flux	LI7500A HMP45AC	CAMPBELL VAISALA			

191

192

193 **3. Data description**

194 **3.1 Near-surface meteorological data (Air temperature, relative humidity, wind speed)**
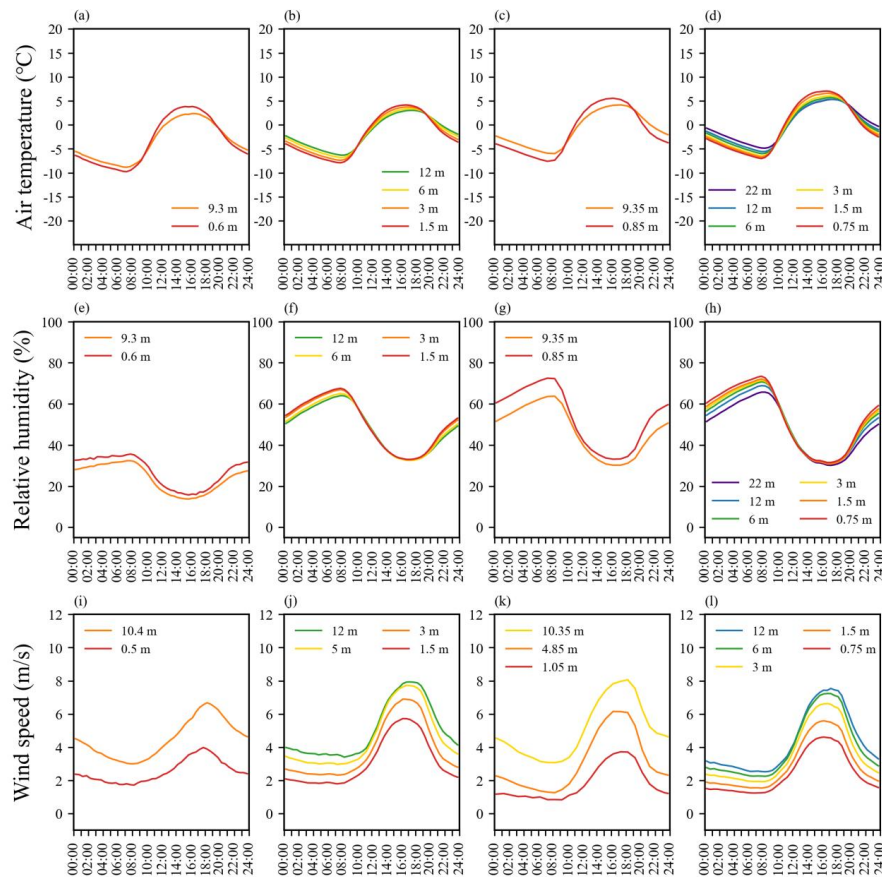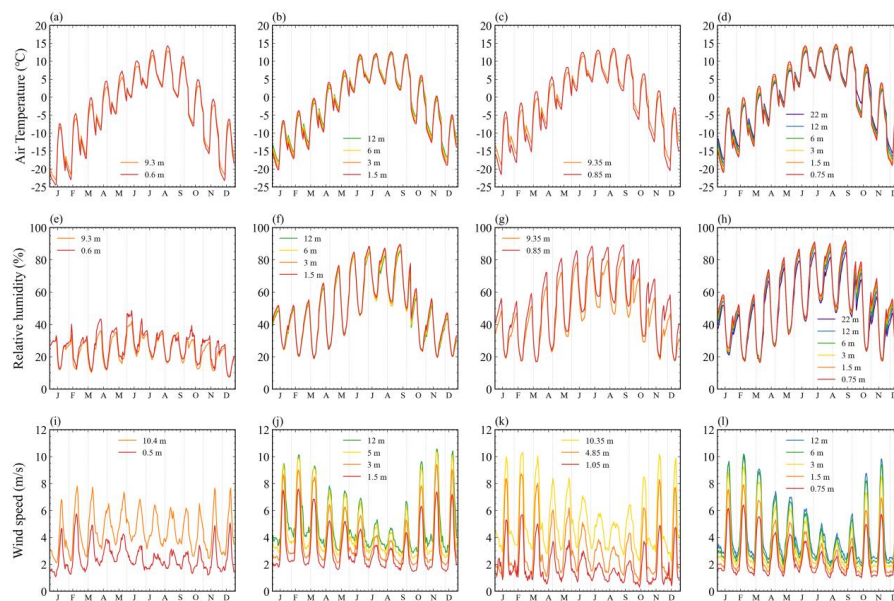
Figure 2. Diurnal variations of temperature at different heights of the PBL tower at NewD66 (a), Amdo (b), MS3478 (c) and BJ (d), with corresponding relative humidity (efgh) and wind speed (ijkl) at each station.

The main variables measured in near-surface micrometeorology are surface temperature, relative humidity and wind speed. Surface air pressure is a single-level observation, which decreases with altitude, while the other variables are gradient observations. Fig. 2 compares the diurnal cycles of temperature, relative humidity and wind speed at different sites to illustrate the micrometeorological characteristics influenced by the different underlying surfaces. Most sites exhibit a maximum temperature at 18:00 and a minimum at 09:00, indicating a clear diurnal pattern. As a result of latitudinal effects, the average temperature at the stations increases from north to south. The northernmost station NewD66 records a minimum temperature of -9.73 °C and a maximum of 3.84 °C, while the southernmost station BJ records a minimum temperature of -7.02 °C and a maximum of 7.05 °C. Irrespective of the water vapour content, relative humidity tends to decrease during the day and increase at night. The most pronounced diurnal variations are observed at lower altitudes. This is because daytime solar radiation heats the surface and atmosphere, making it harder for lower air layers to saturate, which naturally reduces relative humidity. The wind speed generally increases with altitude

213   and shows a diurnal variation, being lower at night and higher during the day. MS3478 is situated in a
214   plateau wetland, where the abundance of vegetation increases friction with the underlying surface,
215   resulting in significantly reduced surface wind speeds at this station in comparison to other
216   locations.

217
218   Figure 3. Monthly diurnal variations of temperature at different heights of the PBL tower at NewD66
219   (a), Amdo (b), MS3478 (c) and BJ (d), with corresponding relative humidity (efgh) and wind speed
220   (ijkl) at each station.
221

222   Most stations exhibited notable seasonal fluctuations in temperature, relative humidity and wind
223   speed (Fig. 3). Due to its cold bareland substrate, the NewD66 station experiences more pronounced
224   diurnal temperature variations, with nighttime temperatures lower than those observed at other stations,
225   occasionally reaching below -20 ℃ in January. In summer, with less pronounced diurnal variations
226   than in winter, temperatures peak at all sites, reaching approximately 13 ℃ during the day and
227   approximately 6 ℃ at night. Diurnal variations in relative humidity also show seasonal patterns, with
228   NewD66 remaining consistently lower, never exceeding 50%, and showing small variations in spring
229   and even smaller variations in summer. In contrast, the most pronounced diurnal variations in relative
230   humidity are observed during the spring at the other stations. As water vapour increases over the
231   plateau, nighttime relative humidity remains above 50% at all sites in summer, with diurnal humidity
232   variations gradually decreasing. Wind speeds show greater diurnal variation in winter and increase with
233   altitude. Peak wind speeds of more than 10 m/s are observed at the Amdo and BJ stations. In summer,
234   the 12 m wind speed at the Amdo and BJ sites peaks at 4.31 m/s in August. Surface wind speeds at
235   MS3478 are consistently low, but upper-level wind speeds are similar to those observed at the other
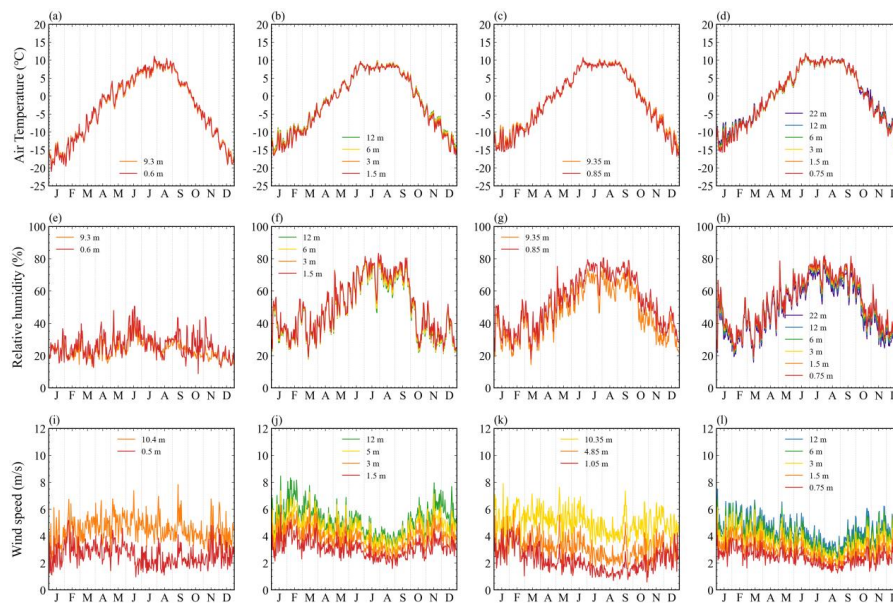236   sites. Consequently, MS3478 exhibits the most pronounced gradient in wind speed.

Figure 4. Daily mean of temperature at different heights of the PBL tower at NewD66 (a), Amdo (b), MS3478 (c) and BJ (d), with corresponding relative humidity (efgh) and wind speed (ijkl) at each station.

Figure 4 presents an annual cycle series, comprising daily mean values derived from gradient observations. At the NewD66 station, winter temperatures are demonstrably lower than at the other stations. In summer, the peak is reached at a later point in time and the duration is shorter. Other stations reach their highest temperatures in June and remain high until early September. With the onset of the monsoon season, continuous water vapour is transported from the ocean to the interior of the TP, resulting in a warming and humidification region. The stations begin to humidify rapidly in early May, reaching a peak in July with daily average relative humidity up to 80%. They then dry rapidly by the end of September, with the end of the monsoon season. The NewD66 station is a plateau bareland, and is only humid for a short period in June, the rest of the year the relative humidity is below 30%. Wind speeds at all stations show a pattern of being lower in summer and higher in winter. The TP is characterised by prevailing westerlies in winter, with daily mean wind speeds reaching 7 m/s. In contrast, the summer months are more humid with frequent changes in weather systems, resulting in average surface wind speeds of less than 4 m/s. Wind speeds at the NewD66 station are lower in winter than at other stations, but higher in summer.

Wind directions at the TP differ significantly between the monsoon and non-monsoon seasons (Fig. 5). Influenced by the South Asian and East Asian summer monsoons, northeast winds dominate during the monsoon season, accounting for 39% of the observations. In winter, there are fewer weather systems and most of the winds are steady westerly winds, with westerly winds accounting for up to 83% of the observations at different stations. MS3478 records different wind directions than the other stations. It has a consistently high frequency of southeast winds in both summer and winter, probably due to the surrounding topography.
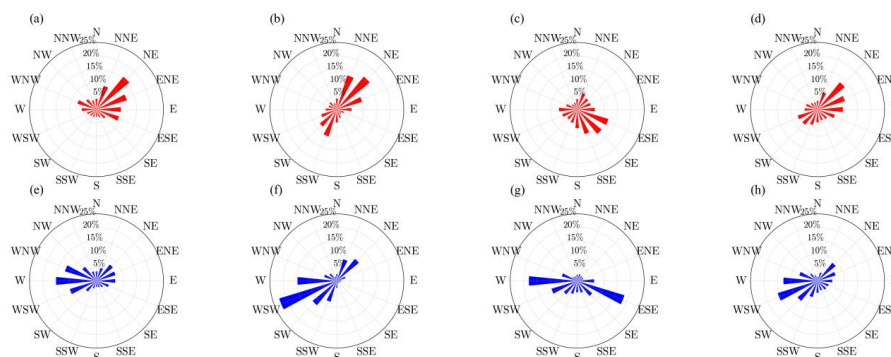
Figure 5. Wind direction during the monsoon season at NewD66 (a), Amdo (b), MS3478 (c), and BJ (d), compared to their wind direction during the non-monsoon season (e-h).

3.2 Radiation fluxes

Downward shortwave radiation (Rsd) is the primary source of energy at the surface, and all stations show similar diurnal patterns of Rsd. Observations indicate that the TP begins to absorb solar radiation at 07:00 and stops completely at 21:00 as the sun sets (Fig. 6). The maximum Rsd occurs in the afternoon and reaches 732 W/m². Seasonal variations demonstrate that Rsd is lowest in winter, increases continuously until spring and peaks in May. This is followed by a decrease during the monsoon season, which is likely due to the effects of frequent summer rainfall on the plateau and cloud cover. Since there is little variation in Rsd, differences in upward shortwave radiation (Rsu) are mainly due to variations in surface albedo. The trend in Rsu at all stations is consistent with that of Rsd, with the highest values observed in May, a decrease during the summer months and the minimum in winter. The start and end times of Rsu at each station align with those of Rsd, as illustrated in Figure 5c. MS3478 and BJ stations exhibit slightly lower Rsu values. MS3478 is plateau wetland, and the area near BJ station is a pasture with extensive vegetation cover in summer, which does not strongly reflect sunlight. Consequently, the lower albedo at these two stations results in relatively lower Rsu values. Longwave radiation is influenced by factors such as water vapour content, aerosol content, temperature stratification and cloud thickness. It shows more pronounced seasonal variations than shortwave radiation. The lowest levels of downward longwave radiation (Rld) are observed in winter, while the highest levels are observed in summer. The diurnal variation of Rld is the smallest of the four radiation components, fluctuating within a range of 45 W/m². Upward longwave radiation (Rlu) is minimal in January, increases steadily until June, and stabilises at 370 W/m² during the summer months (June to August). At station MS3478, Rlu is relatively lower, remaining around 350 W/m² during the summer. The minimum of Rlu occurs at 08:00, coinciding with the lowest surface temperatures. The maximum values occur in the afternoon and show greater diurnal variations compared to Rld, with fluctuations up to 140 W/m². Net surface radiation exhibits a clear diurnal cycle, with peaks in the afternoon and slightly negative values at night. This highlights the process of surface heating the atmosphere during the day and cooling it at night. Annual variations show that net surface radiation is highest in summer and lowest in winter.
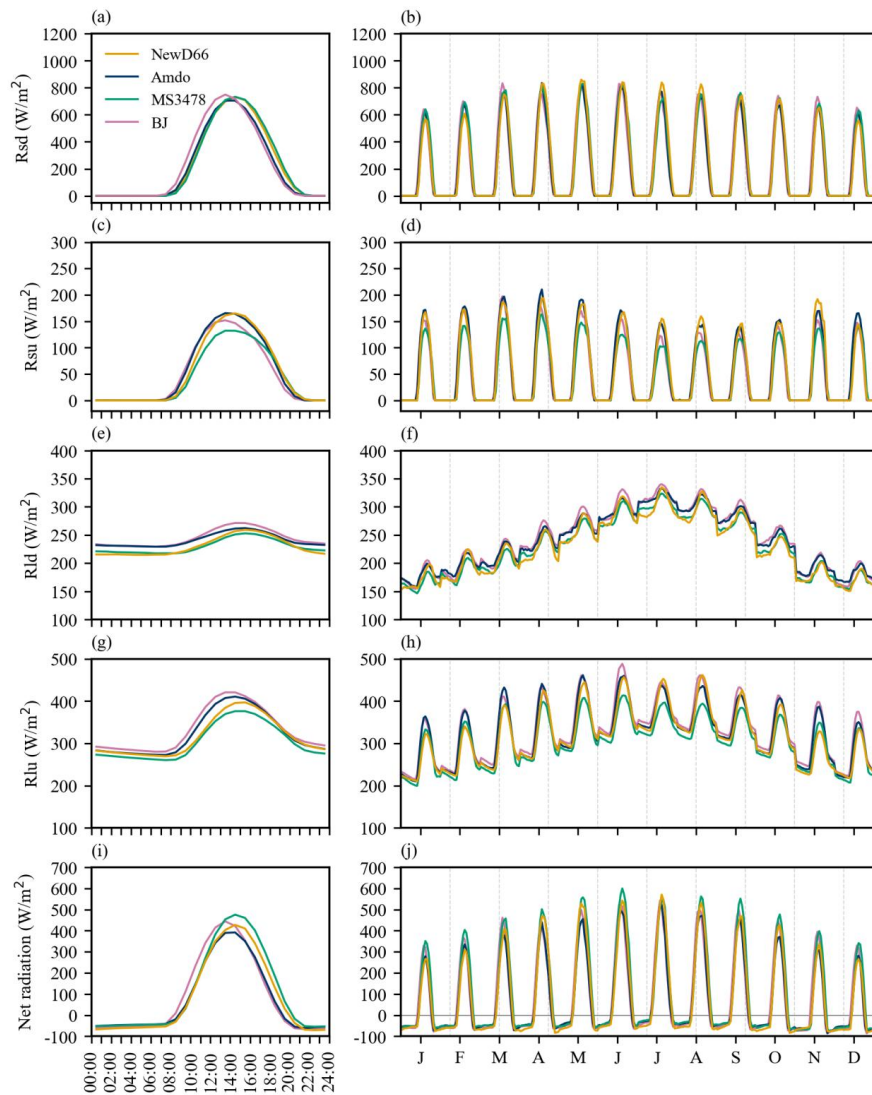
Figure 6. Diurnal variations (the first column) and monthly variations of the diurnal (the second column) downward shortwave radiation (a-b), upward shortwave radiation (c-d), downward longwave radiation (e-f), upward longwave radiation (g-h) ,and net radiation (i-j) at the 4 stations.

3.3 Sensible heat and latent heat fluxes

Sensible heat flux (SH) and latent heat flux (LH) are the primary forms of energy transfer between the surface and the atmosphere. Fig. 7 illustrates the monthly diurnal cycles and annual variations of SH and LH at each station. SH is influenced by the temperature difference between the surface and the atmosphere, as well as weather systems associated with precipitation, leading to numerous transient fluctuations. Seasonal variations demonstrate stronger SH at each station in spring and weaker in

303   summer. The daily peaks occur at 14:00, with negative values at night in winter, indicating clear

304   temperature inversions. While net radiation increases steadily in spring, the energy absorbed by the

305   surface before March is mainly used to melt snow. The onset of the monsoon season in May is

306   accompanied by a rapid increase in water vapour on the TP, with a gradual dominance of LH transfer.

307   Consequently, SH peaks in April at each station, with MS3478 (a plateau wetland) peaking in February.

308   The Asian monsoon system transports substantial moisture into the plateau during the summer,

309   resulting in low peaks in sensible heat flux at all stations, with a daily average of 20 W/m². In summer,

310   the NewD66 station experiences the highest SH, while the MS3478 station experiences the lowest SH,

311   reflecting the differences in water vapour content between the plateau bareland and plateau wetland.
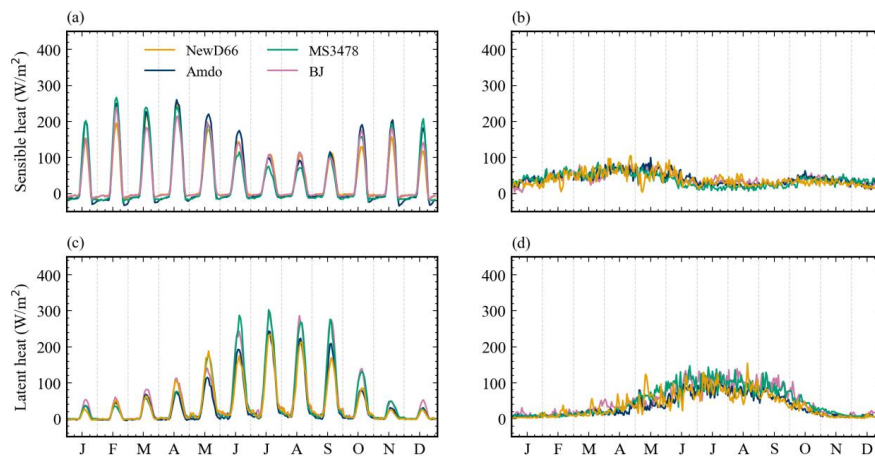

312

313   Figure 7. Monthly variations of the diurnal (the first column) and daily mean (the second column)

314   sensible heat (a-b), latent heat (c-d), and total heat flux (e-f) at the 4 stations.

315

316   The seasonal variation trend of LH is in opposition to that of SH. During the winter, the plateau is

317   characterised by a relatively cold and dry climate, with LH peaks not exceeding 60 W/m² at all stations.

318   As the monsoon season commences in May, LH rapidly rises, maintaining levels above 100 W/m²

319   throughout the summer until it begins to decline in October. Peaks in LH occur in July at all stations,

320   with MS3478's peak appearing earlier in June due to its higher moisture content and remaining high

321   throughout the summer. In winter, nighttime LH approaches zero, but retains weak positive values in

322   summer, indicating that no clear temperature inversions occur at night, and even contributing to heating

323   the atmosphere in the early hours of the night. Fig. 7d shows significant fluctuations in LH during the

324   summer months, which are attributed to the frequent alterations in weather patterns. The diurnal cycle

325   of LH is also influenced by the occurrence of extreme rainfall episodes.
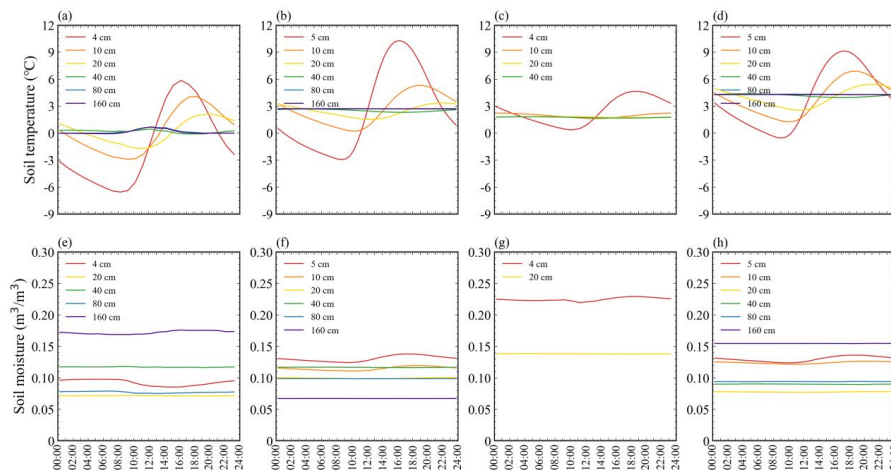
326   **3.4 Soil hydrothermal characteristics**

Figure 8. Layered soil temperature at NewD66 (a), Amdo (b), MS3478 (c), and BJ (d) observation, and corresponding layered soil moisture (efgh) at each station.

Soil thermal and moisture variations have a significant impact on energy and moisture exchange between the surface and the atmosphere. Due to varying observation conditions, soil observation depths differ between stations. Fig. 8 shows that all stations exhibit a diurnal cycle in soil temperature, with cooling at night and warming during the day. Soil temperature variation diminishes with increasing depth, with 4cm, 10cm, and 20cm depths showing a 2-hour delay in heating and cooling cycles. Significant spatial variation is observed due to differences in soil type, porosity, and substrate. The soil temperature at NewD66 station tends to be lower than at other sites, with 4-cm depths reaching a minimum of -6.56 °C at night. This is due to a lack of moisture in the surrounding air, which results in a greater daily heating effect, reaching 5.86 °C by 16:00. At 160 cm, a slight midday fluctuation is observed, which is not seen at other stations. MS3478, a plateau wetland, exhibits a diurnal variation of 4.29 °C at 4-cm depth, with a slight rise at 10 cm at 22:00, and minimal diurnal variation below 10 cm.

The diurnal cycle of soil moisture is weak at the shallowest layer, with fluctuations not exceeding 0.015 m³/m³. Below 10 cm, soil moisture shows no clear diurnal cycle. The overall soil moisture at NewD66 station is relatively low, but it does not vary linearly with depth. For example, 5-cm depth soil moisture is 0.09 m³/m³, while 160-cm depth moisture remains consistently at 0.17 m³/m³. The soil moisture data from the BJ station exhibits a comparable pattern, with slight fluctuations at the 5-cm depth, maintaining an average of approximately 0.13 m³/m³, and negligible variation at the 160-cm depth, remaining at 0.15 m³/m³. In contrast, the soil moisture at the 160-cm depth from Amdo is considerably lower than that observed in the shallow layers, likely due to the presence of a permafrost layer, which results in a consistently low liquid water content. MS3478's soil moisture exhibits no significant diurnal variation, with 4-cm depth soil moisture averaging 0.22 m³/m³ and 20-cm depth soil moisture averaging 0.13 m³/m³, which are both significantly higher than those observed at other stations.
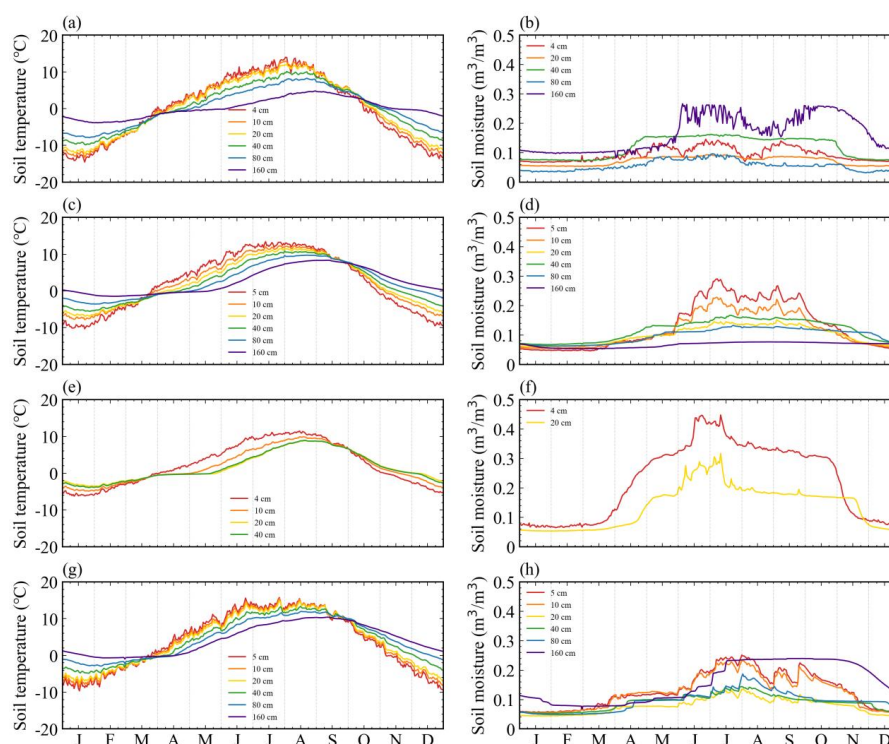
Figure 9. Daily mean soil temperature (a) and soil moisture (b) at NewD66,
same in Amdo (cd), MS3478 (ef), and BJ (gh).

Soil temperature and moisture exhibit clear annual variations at each station, with soil temperature delaying more with increasing observation depth (Fig. 9). Surface soil temperatures peak in July, 40-cm depth temperatures in August, and 160-cm depth temperatures in September. The greatest annual variation in soil temperature is observed in NewD66's 4-cm depth soil temperature, reaching 28.56 ℃, while the smallest is observed in MS3478's, at 17.74 ℃. A similar trend is observed in soil moisture, with higher levels observed in summer and lower levels in winter. Soil moisture increases in spring due to the melting of snow and ice, and in summer due to precipitation. In the absence of rainfall, surface evaporation and runoff results in a rapid decrease in soil moisture. There are significant differences in soil moisture between stations, with substantial fluctuations in surface moisture, indicating vertical variation in the soil moisture profile. NewD66's 4-cm depth soil moisture exhibits minimal annual variation, increasing by only 0.05 m³/m³ in summer. However, 160-cm depth moisture rapidly increases to 0.24 m³/m³ in summer, then gradually decreases in November, coinciding with the point at which 160-cm depth soil temperatures exceed 0 ℃. The soil moisture at all layers of Amdo is below 0.1 m³/m³ in winter, with 5-cm depth moisture reaching 0.29 m³/m³ in summer, and decreasing with increasing depth. MS3478's humid air contributes to higher soil moisture, with 4-cm depth moisture maintaining levels above 0.3 m³/m³ from May to October, even exceeding 0.8 m³/m³ at times. BJ's 4-cm depth moisture rises in April, peaking in August at 0.25 m³/m³. The lowest 20-cm depth moisture is observed year-round, at only 0.12 m³/m³ in July. The 160-cm depth moisture rapidly rises in June, maintaining 0.24 m³/m³ until November.

376

4. Data availability

378   Near-surface micrometeorology, soil hydrothermal characteristics, and turbulent flux observation
379 datasets are openly available at https://doi.org/10.11888/Meteoro.tpdc.270010 (Hu et al., 2019) and
380 https://doi.org/10.11888/Atmos.tpdc.300325 (Wang et al., 2023). Following a rigorous screening
381 process that included the identification and elimination of missing values, the physical range check,
382 and the manual quality control, valid data in CSV format is available for download. The file names
383 adhere to the convention of station_datatype_year.csv, and all data files utilise UTC+8 as the
384 designated time standard. Each CSV-formatted data file name includes the name of the variable, the
385 observed height/depth, and the unit.

386

5. Conclusion and Discussion

388   As demonstrated in previous sections, the NPCE reliably reflects the characteristics of various
389 variables across different underlying surface and temporal scales, thereby showcasing the reliability
390 and completeness of the data. The challenging environment and dispersed stations on the CTP make it
391 difficult to maintain equipment, which makes the data collected valuable. The scarcity of field
392 observation data has long been a barrier to in-depth research on the TP. Thus, long-term observations
393 and scientific data sharing are crucial for research on the plateau. This paper introduces land-
394 atmosphere interaction data from several observation stations centred around Nagqu. The dataset
395 comprises 9 years (2014-2022) of hourly continuous series of near-surface meteorological, radiation,
396 turbulent flux, and soil hydrothermal characteristics. This enables effective exploration of the entire
397 process of land-atmosphere interactions on the plateau. Additionally, all data were manually checked
398 for outliers and subjected to quality control. The long-term half-hourly dataset from NPCE provides the
399 opportunity to conduct high-precision numerical simulations at the local level. This enables in-depth
400 research to be conducted on the mechanisms by which the land and atmosphere interact on the plateau
401 and also provides support for comprehensive research into the plateau's energy and water cycles and
402 climate change.

403   The NPCE is a comprehensive research platform with the primary goal of observing and studying
404 the impacts of weather and climate change on the Tibetan Plateau, water resource utilisation, ecological
405 environmental protection, and human activities. The main objective of the NPCE is based on a plateau
406 climate and the water-energy cycle. In recent years, a range of processes have been the focus of
407 detailed analysis, including non-homogeneous terrain turbulence transfer mechanisms, radiation
408 balance components and energy allocation processes. The analysis has been informed by long-term in
409 situ meteorological observations (Huang et al., 2016). The spatial and temporal variability of SH and
410 LH under complex topographic forcing is a particular highlight (Xie et al., 2018), and energy closure in
411 the central part of the northern Tibetan plateau is further discussed (Li et al., 2015; Li et al., 2016).
412 Satellite-derived products have been utilised to address the spatial representation limitations inherent in
413 field observations (Ma et al., 2014; Ma et al., 2009; Ma et al., 2006). Furthermore, ground-based
414 observations were utilised to validate and calibrate the remote sensing estimates of sensed LH, thereby
415 improving the accuracy of the remote sensing algorithms (Zhong et al., 2019). A distributed sensor
416 network was utilised to monitor soil temperature and humidity gradients, thereby enabling the
417 systematic quantification of the disparities in soil moisture and heat fluxes between permafrost and
418 seasonal permafrost. In these areas, phase change LH associated with freeze-thaw transitions have been
419 demonstrated to influence surface energy distribution (Liu et al., 2015; Fu et al., 2022). A

420 comprehensive analysis of the pattern of boundary layer changes on the CTP has been conducted
421 utilising PBL towers, as well as MWR and radiosonde data (Wang et al., 2025; Sun et al., 2021;
422 Sun et al., 2020). The integration of multi-source observations (Near-surface meteorological data, EC
423 system, boundary layer observation, and satellite inversion) has modified the model representation of
424 land-atmosphere energy balance processes, and further refinement of the parameterisation scheme has
425 been applied to soil freeze-thaw processes (Deng et al., 2021). The enhanced numerical simulation
426 accuracy of blowing snow processes in the CLM model facilitates a more profound comprehension of
427 surface processes and cryosphere changes in local area (Xie et al., 2023; Xie et al., 2021).

428 The data presented in the paper is the average result after filtering out missing values. However, in
429 practical applications, considering the difficulty of instrument maintenance, there may inevitably be
430 anomalies or data discontinuities. As a key observation project on the CTP, the NPCE is implementing
431 an ambitious plan to enhance its monitoring capabilities for understanding global climate dynamics due
432 to its high altitude and ecological sensitivity. This initiative focuses on acquiring advanced
433 instrumentation and expanding monitoring sites to deepen insights into atmospheric, hydrological, and
434 ecological processes, particularly in the CTP and the upper Nu River (Salween River) basin. For
435 instrument acquisition, the station will deploy Raman lidar systems, which are highly specialized for
436 simultaneous detection of water vapor and aerosols in the lower atmosphere. These Raman lidar
437 systems utilize laser-based spectroscopy to provide high-resolution measurements of water vapor
438 concentrations, enabling detailed analysis of moisture transport and its influence on regional climate
439 patterns. Additionally, the same Raman lidar systems will measure aerosol properties, such as particle
440 size, concentration, and distribution, which are essential for studying air quality, aerosol-cloud
441 interactions, and their impact on radiative forcing in the plateau's unique environment. To complement
442 these atmospheric measurements, the station will acquire advanced greenhouse gas analyzers
443 specifically designed to monitor carbon dioxide and methane fluxes from soil and vegetation
444 respiration, providing critical data on biogeochemical cycles and the carbon dynamics of high-altitude
445 ecosystems under changing climatic conditions.

446 The site expansion plan involves establishing new monitoring stations on the CTP and the upper Nu
447 River basin to broaden the scope of environmental observations. The CTP, with its expansive high-
448 altitude grasslands, offers a unique setting to study the interplay between atmospheric processes and
449 ecosystem responses to climate change. Similarly, the upper Nu River basin, a vital hydrological region,
450 will host new sites to investigate water cycles, soil moisture dynamics, and vegetation responses to
451 environmental shifts. By expanding coverage in the upstream Nu River, the station aims to capture
452 spatial and temporal variations in hydrological and ecological parameters, supporting research on water
453 resource management, ecosystem resilience, and climate adaptation strategies in this ecologically
454 sensitive area.

455
456

464
465   **References**
466
467   Bian, L., Gao Z., Ma Y., Koike T., Ma Y., Li Y., Sun J., Hu Z. and Xu X.: Seasonal Variation in
468   Turbulent Fluxes over Tibetan Plateau and Its Surrounding Areas: Research Note, Journal of
469   the Meteorological Society of Japan., 90C, 157-171, 2012.
470   Ciwangdunzhu, Du J. and Danzengcuojie: Spatial-temporal Change of Consecutive Dry Days in
471   Changtang National Nature Reserve of Tibet During 1971-2017, Chinese Agricultural Science
472   Bulletin, 34(30),118-122, 2018. (in Chinese).
473   Chen, B., Chao W. and Liu X.: Enhanced climatic warming in the Tibetan plateau due to doubling CO_2:
474   A model study, Climate Dynamics, 20(4), 401–413, 2003.
475   Curio, J. and Scherer D.: Seasonality and spatial variability of dynamic precipitation controls on the
476   Tibetan Plateau, Earth System Dynamics, 7(3), 767-782, 2016.
477   Deng, M., Meng X., Lu Y., Li Z., Zhao L., Hu Z., Chen H., Shang L., Wang S. and Li Q.: Impact and
478   sensitivity analysis of soil water and heat transfer parameterizations in Community Land
479   Surface Model on the Tibetan Plateau, Journal of Advances in Modeling Earth Systems, 13(9),
480   e2021MS002670, 2021.
481   Duan, A. and Xiao Z.: Does the climate warming hiatus exist over the Tibetan Plateau? Scientific
482   reports 5(1), 13711, 2015.
483   Fan, X., Li Y. and Li L.: Synoptic-Scale Effects of Atmospheric Heat Source over Key Areas of the
484   Tibetan Plateau on Its Downstream Rainfall in Summer, Journal of Climate, 36(11), 3647-
485   3666, 2023.
486   Fu, C., Hu Z., Yang Y., Deng M., Yu H., Lu S., Wu D. and Fan W.: Responses of Soil Freeze-Thaw
487   Processes to Climate on the Tibetan Plateau from 1980 to 2016, Remote Sensing, 14(23),
488   5907, 2022.
489   Gu, L., Yao J., Hu Z. and Zhao L.: Comparison of the surface energy budget between regions of
490   seasonally frozen ground and permafrost on the Tibetan Plateau, Atmospheric Research, 153,
491   553-564, 2015.
492   Gu, L., Yao J., Hu Z., Ma Y., Sun F., Yu H., Wang S., Yang Y., Guo R. and Qin Y.: Characteristics of
493   the atmospheric boundary layer's structure and heating (cooling) rate in summer over the
494   Northern Tibetan Plateau, Atmospheric Research, 269, 106045, 2022.
495   Guo, Y., Zhang Y., Ma Y., Ma N.: Surface heat source intensity and surface water/energy balance in
496   Shuanghu, northern Tibetan Plateau, Acta Geographica Sinica, 69(07),983-992, 2014.
497   He, H., Hu Z., Xun X., Hao L., Gu L., Sun J. and Xu L.: The variation characteristics of surface
498   radiation in wetlands on the northern Tibetan Plateau, Acta Energiae Solaris Sinica,
499   31(05),561-567, 2010. (in Chinese).
500   Hu, Z., Gu, L., Sun, F., Wang, S. Dataset of meteorological elements of Nagqu Station of Plateau
501   Climate and Environment (2014-2017) [data set]. National Tibetan Plateau / Third Pole
502   Environment Data Center. https://doi.org/10.11888/Meteoro.tpdc.270010, 2019.
503   Huang, F. and Ma W.: Analysis of Long-Term Meteorological Observation for Weather and Climate
504   Fundamental Data over the Northern Tibetan Plateau, Advances in Meteorology, 2016(1),
505   4878353, 2016.
506   Immerzeel, W., Lutz A., Andrade M., Bahl A., Biemans H., Bolch T., Hyde S., Brumby S., Davies B.,
507   Elmore A., Emmer A., Feng M., Fernández A., Haritashya U., Kargel J., Koppes M.,

508   Kraaijenbrink P., Kulkarni A., Mayewski P., Nepal S., Pacheco P., Painter T., Pellicciotti F.,
509   Rajaram H., Rupper S., Sinisalo A., Shrestha A., Viviroli D., Wada Y., Xiao C., Yao T. and
510   Baillie J.: Importance and vulnerability of the world's water towers, Nature, 577(7790), 364-
511   369, 2020.

512   Immerzeel, Van Beek L. and Bierkens M.: Climate change will affect the Asian water towers, science,
513   328(5984), 1382-1385, 2010.

514   Jin, H., He R., Cheng G., Wu Q., Wang S., Lü L. and Chang X.: Changes in frozen ground in the
515   Source Area of the Yellow River on the Qinghai–Tibet Plateau, China, and their eco-
516   environmental impacts, Environmental Research Letters, 4(4), 045206, 2009.

517   Kang, S., Xu Y., You Q., Flügel W., Pepin N. and Yao T.: Review of climate and cryospheric change
518   in the Tibetan Plateau, Environmental research letters, 5(1), 015101, 2010.

519   Lei, Y., Yang K., Wang B., Sheng Y., Bird B., Zhang G. and Tian L.: Response of inland lake
520   dynamics over the Tibetan Plateau to climate change, Climatic Change, 125, 281-290, 2014.

521   Lei, Y., Yao T., Bird B., Yang K., Zhai J. and Sheng Y.: Coherent lake growth on the central Tibetan
522   Plateau since the 1970s: Characterization and attribution, Journal of Hydrology, 483, 61-67,
523   2013.

524   Li, L., Liu Q., Zhang Y., Liu L., Ding M. and Gu C.: Spatial distribution and variation of precipitation
525   in the Qiangtang Plateau, Geographical Research, 36(11),2047-2060, 2017. (in Chinese)

526   Li, G., Chen H., Xu M., Zhao C., Zhong L., Li R., Fu Y. and Gao Y.: Impacts of topographic
527   complexity on modeling moisture transport and precipitation over the Tibetan Plateau in
528   summer, Advances in Atmospheric Sciences, 39(7), 1151-1166, 2022.

529   Li, M., Babel W., Chen X., Zhang L., Sun F., Wang B., Ma Y., Hu Z. and Foken T.: A 3-year dataset
530   of sensible and latent heat fluxes from the Tibetan Plateau, derived using eddy covariance
531   measurements, Theoretical and Applied Climatology, 122(3-4), 457-469, 2015.

532   Li, M., Su Z., Ma Y., Chen X., Zhang L. and Hu Z.: Characteristics of land-atmosphere energy and
533   turbulent fluxes over the plateau steppe in central Tibetan Plateau, Sciences in cold and arid
534   regions, 8(2), 103-115, 2016.

535   Li, W., Guo W., Qiu B., Xue Y., Hsu P. and Wei J.: Influence of Tibetan Plateau snow cover on East
536   Asian atmospheric circulation at medium-range time scales, Nature communications, 9(1),
537   4243, 2018.

538   Li, Y. and Hu Z.: A Study on Parameterization of Surface Albedo over Grassland Surface in the
539   Northern Tibetan Plateau, Advances in Atmospheric Sciences, 26(1), 161-168, 2009.

540   Liu, H., Hu Z., Yang Y., Wang Y., Sun G. and Huang R.: Simulation of the freezing-thawing processes
541   at Nagqu Area over Qinghai-Xizang Plateau, Plateau Meteorology, 34(003), 676-683, 2015.

542   Liu, X. and Chen B.: Climatic warming in the Tibetan Plateau during recent decades, International
543   Journal of Climatology: A Journal of the Royal Meteorological Society, 20(14), 1729-1742,
544   2000.

545   Liu, X., Cheng Z., Yan L. and Yin Z.: Elevation dependency of recent and future minimum surface air
546   temperature trends in the Tibetan Plateau and its surroundings, Global and Planetary Change,
547   68(3), 164–174, 2009.

548   Ma, W., Ma Y., Li M., Hu Z., Zhong L., Su Z., Ishikawa H. and Wang J.: Estimating surface fluxes
549   over the north Tibetan Plateau area with ASTER imagery, Hydrology and earth system
550   sciences, 13(1), 57-67, 2009.

551　Ma, Y., Wang Y. and Han C.: Regionalization of land surface heat fluxes over the heterogeneous
552　　　　landscape: from the Tibetan Plateau to the Third Pole region, International Journal of Remote
553　　　　Sensing, 39(18), 5872-5890, 2018.

554　Ma, Y., Xie Z., Chen Y., Liu S., Che T., Xu Z., Shang L., He X., Meng X., Ma W., Xu B., Zhao H.,
555　　　　Wang J., Wu G. and Li X.: Spatially extensive long-term quality-assured land-atmosphere
556　　　　interactions dataset over the Tibetan Plateau, Earth System Science Data Discussions, 2024, 1-
557　　　　37, 2023.

558　Ma, Y., Yao T., Zhong L., Wang B., Xu X., Hu Z., Ma W., Sun F., Han C., Li M., Chen X., Wang J.,
559　　　　Li Y., Gu L., Xie Z., Liu L., Sun G., Wang S., Zhou D., Zuo H., Xu C., Liu X., Wang Y. and
560　　　　Wang Z.: Comprehensive study of energy and water exchange over the Tibetan Plateau: A
561　　　　review and perspective: From GAME/Tibet and CAMP/Tibet to TORP, TPEORP, and
562　　　　TPEITORP, Earth-Science Reviews, 237, 104312, 2023.

563　Ma, Y., Zhong L., Su Z., Ishikawa H., Menenti M. and Koike T.: Determination of regional
564　　　　distributions and seasonal variations of land surface heat fluxes from Landsat-7 Enhanced
565　　　　Thematic Mapper data over the central Tibetan Plateau area, Journal of Geophysical Research:
566　　　　Atmospheres, 111(D10), 2006.

567　Qiu, J.: China: the third pole, Nature, 454(7203), 393-397, 2008.

568　Shen, M., Piao S., Jeong S., Zhou L., Zeng Z., Ciais P., Chen D., Huang M., Jin C., Li L., Li Y.,
569　　　　Myneni R., Yang K., Zhang G., Zhang Y. and Yao T.: Evaporative cooling over the Tibetan
570　　　　Plateau induced by vegetation growth, Proceedings of the National Academy of Sciences,
571　　　　112(30), 9299-9304, 2015.

572　Shen, Y. and Xiong A.: Validation and comparison of a new gauge-based precipitation analysis over
573　　　　mainland China, International journal of climatology, 36(1), 252-265, 2016.

574　Song, C., You S., Ke L., Liu G. and Zhong X.: Phenological variation of typical vegetation types in
575　　　　northern Tibet and its response to climate changes, Acta Ecol. Sin, 04, 41–51, 2012.

576　Sun, C., Xu X., Wang P., Yang D., Zhang S., Wang C. and Cai W.: The warming and wetting
577　　　　ecological environment changes over the Qinghai-Tibetan Plateau and the driving effect of the
578　　　　Asian summer monsoon, Journal of Tropical Meteorology, 28(1), 95-108, 2022.

579　Sun, G., Hu Z., Ma Y., Xie Z., Wang J. and Yang S.: Simulation Analysis of Local Land Atmosphere
580　　　　Coupling in Rainy Season over a Typical Underlying Surface in the Tibetan Plateau,
581　　　　Hydrology and Earth System Sciences, 24, 5937–5951, 2020.

582　Sun, G., Hu Z., Ma Y., Xie Z., Yang S. and Wang J.: Analysis of local land-atmosphere coupling in
583　　　　rainy season over a typical underlying surface in Tibetan Plateau based on field measurements
584　　　　and ERA5, Atmospheric Research, 243, 105025, 2020.

585　Sun, G., Hu Z., Ma Y., Xie Z., Sun F., Wang J. and Yang S.: Analysis of local land atmosphere
586　　　　coupling characteristics over Tibetan Plateau in the dry and rainy seasons using observational
587　　　　data and ERA5, Science of the Total Environment, 774, 145138, 2021.

588　Sun, J., Yang K., Guo W., Wang Y., He J. and Lu H.: Why has the inner Tibetan Plateau become
589　　　　wetter since the mid-1990s? Journal of Climate, 33(19), 8507-8522, 2020.

590　Ueno, K., Sugimoto S., Tsutsui H., Taniguchi K., Hu Z. and Wu S.: Role Of Patchy Snow Cover On
591　　　　The Planetary Boundary Layer Structure During Late Winter Observed In The Central Tibetan
592　　　　Plateau, Journal of The Meteorological Society of Japan, 90c, 145-155, 2012.

593 Wang, G., Hu Z., Yu H., Sun G., Niu R. and Wang X.: Land-atmosphere coupling characteristics in
594   summer based on microwave radiometer data at Nagqu site of Tibetan Plateau, Atmospheric
595   Research, 320, 108074, 2025.

596 Wang, S., Hu, Z., Gu, L., Sun, F. Comprehensive observation data set of multi-sphere land-atmosphere
597   interaction at 8 sites in the westerly zone and monsoon zone from 2018 to 2022 [data set].
598   National Tibetan Plateau / Third Pole Environment Data
599   Center. https://doi.org/10.11888/Atmos.tpdc.300325, 2023.

600 Wu, G., Liu Y., Zhang Q., Duan A., Wang T., Wan R., Liu X., Li W., Wang Z. and Liang X.: The
601   influence of mechanical and thermal forcing by the Tibetan Plateau on Asian climate, Journal
602   of Hydrometeorology, 8(4), 770-789, 2007.

603 Wu, G., Liu Y., He B., Bao Q., Duan A. and Jin F.: Thermal Controls on the Asian Summer Monsoon,
604   Scientific reports, 2(1), 404, 2012.

605 Xie J., Yu Y., Liu C. and Ge J.: Characteristics of Surface Sensible Heat Flux over the Qinghai-Tibetan
606   Plateau and Its Response to Climate Change, Plateau Meteorology, 37(1), 28-42, 2018.

607 Xie, Z., Ma W., Ma Y., Hu Z., Sun G., Han Y., Hu W., Su R. and Fan Y.: "Decision tree-based
608   detection of blowing snow events in the European Alps, Hydrology and earth system sciences,
609   25(7), 3783-3804, 2021.

610 Xie, Z., Ma Y., Ma W., Hu Z. and Sun G.: Comparison of varied complexity parameterizations in
611   estimating blowing snow occurrences, Journal of Hydrology, 619, 129291, 2023.

612 Yang, K., He J., Tang W., Qin J. and Cheng C.: On downward shortwave and longwave radiations over
613   high altitude regions: Observation and modeling in the Tibetan Plateau, Agricultural and
614   Forest Meteorology, 150(1), 38-46, 2010.

615 Yang K., Koike T., Fujii H., Tamagawa K. and Hirose N.: Improvement of Surface Flux
616   Parameterizations with a Turbulence-Related Length, Quarterly Journal of Royal
617   Meteorological Society, 128(584), 2073-2087, 2002.

618 Yang, K., Wu H., Qin J., Lin C., Tang W. and Chen Y.: Recent climate changes over the Tibetan
619   Plateau and their impacts on energy and water cycle: A review, Global and Planetary Change,
620   112, 79-91, 2014.

621 Yang, K., Ye B., Zhou D., Wu B., Foken T., Qin J. and Zhou Z.: Response of hydrological cycle to
622   recent climate changes in the Tibetan Plateau, Climatic change, 109, 517-534, 2011.

623 Yao, T., Thompson L., Yang W., Yu W., Gao Y., Guo X., Yang X., Duan K., Zhao H., Xu B., Pu J., Lu
624   A., Xiang Y., Kattel D. and Joswiak D.: Different glacier status with atmospheric circulations
625   in Tibetan Plateau and surroundings, Nature climate change, 2(9), 663-667, 2012.

626 Zhang, G., Luo W., Chen W. and Zheng G.: A robust but variable lake expansion on the Tibetan
627   Plateau, Science Bull, 64(18), 1306-1309, 2019.

628 Zhang, T., Wang T., Krinner G., Wang X., Gasser T., Peng S., Piao S. and Yao T.: The weakening
629   relationship between Eurasian spring snow cover and Indian summer monsoon rainfall,
630   Science advances, 5(3), eaau8932, 2019.

631 Zhao, Y., Xu X., Liu L., Zhang R., Xu H., Wang Y. and Li J.: Effects of convection over the Tibetan
632   Plateau on rainstorms downstream of the Yangtze River Basin, Atmospheric Research, 219,
633   24-35, 2019.

634 Zhong, L., Zou M., Ma Y., Huang Z., Xu K., Wang X., Ge N. and Cheng M.: Estimation of
635   downwelling shortwave and longwave radiation in the Tibetan Plateau under all-sky
636   conditions, Journal of Geophysical Research: Atmospheres, 124(21), 11086-11102, 2019.

637   Zou, M., Zhong L., Ma Y., Hu Y. and Feng L.: Estimation of actual evapotranspiration in the Nagqu
638   river basin of the Tibetan Plateau, Theoretical and Applied Climatology, 132(3-4), 1039-1047,
639   2018.
640